ENERGY CASCADE SUSTAINING TURBULENCE IN A PRECESSING SPHERE

Yasufumi Horimoto

Graduate School of Engineering Science
Osaka University
1-3 Machikaneyama, Toyonaka, Osaka, 560-8531 Japan
y_horimoto@fm.me.es.osaka-u.ac.jp

Susumu Goto

Graduate School of Engineering Science
Osaka University
1-3 Machikaneyama, Toyonaka, Osaka, 560-8531 Japan
goto@me.es.osaka-u.ac.jp

ABSTRACT

Fully developed turbulence is sustained in a precessing sphere when the Reynolds number is sufficiently high and the precession rate (the Poincaré number) is about 0.1. We experimentally investigate the sustaining mechanism of this developed turbulence. Our strategy of the investigation is using a dilute surfactant solution, which is a non-Newtonian fluid with viscoelasticity, and comparing turbulence of the surfactant solution with water turbulence under the common flow conditions. Flow visualizations show that small-scale turbulent eddies are strongly suppressed by the viscoelasticity. This is the case for all the examined Reynolds numbers; whereas particle image velocimetry (PIV) shows that large-scale vortices are suppressed only when the Reynolds number is high enough so that their time-scale may be comparable with the characteristic time-scale of the viscoelasticity. The combination of these experimental results and previous studies on the mechanism of turbulence suppression shows that small-scale turbulent eddies in the precessing sphere are sustained through an energy cascading process rather than the simple advection from a high-shear-rate region near the wall.

BACKGROUND & PURPOSE

The word "precession" denotes the rotation of the spin axis of a rotating object about another axis (Fig. 1). Half a century ago, Malkus (1968) experimentally showed that a slowly precessing container can sustain turbulence of a confined fluid. Many geophysicists have been interested in this fact because the Earth's precession may lead to the dynamo due to turbulent motion of molten iron in the outer core of the Earth (Le Bars et al., 2015). We are interested in this fact from another viewpoint. Since a precessing container is a useful table-top turbulence generator, it is likely to have many engineering applications. For example, we are constructing a mixer without stirring blades using a precessing container.

In the present study, we investigate turbulence in a precessing *sphere* where the axes of the spin and precession are at a right angle. Note that, once the angle between the two axes is fixed, flows in a precessing sphere are controlled only by two dimensionless parameters: the Reynolds number and the Poincaré number defined by

$$Re = \frac{a^2 \Omega_s}{\nu}, \qquad (1)$$

and,

$$Po = \frac{\Omega_p}{\Omega_s}. \qquad (2)$$

Here, a is the radius of the sphere, ν is the kinematic viscosity of a confined fluid, Ω_s and Ω_p are the magnitudes of the angular velocities of the spin and precession, respectively.

In our previous experimental and numerical studies on flows in a precessing sphere (Goto et al., 2014a, 2014b), we have shown the following. (i) Mean flow structures are predominantly determined by the Poincaré number, and they are almost independent of the Reynolds number. (ii) For a fixed Reynolds number, the most developed turbulence is sustained when $Po \approx 0.1$. (iii) Our direct numerical simulations (DNS) show that there exists a pair of large-scale vortex tubes in the turbulence for $Po = 0.1$ and $Re = O(10^4)$ (Fig. 2).

Thus we have successfully revealed the parameter dependence of the statistics and large-scale flow structures of the turbulence in a precessing sphere. However, there remains an open question: how is the turbulence sustained in the smooth cavity? The purpose of the present paper is to answer this question.
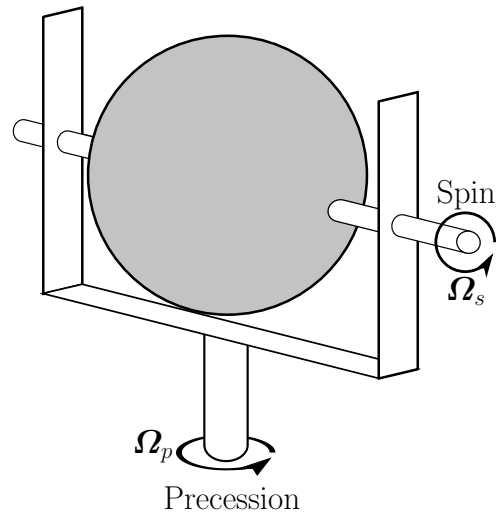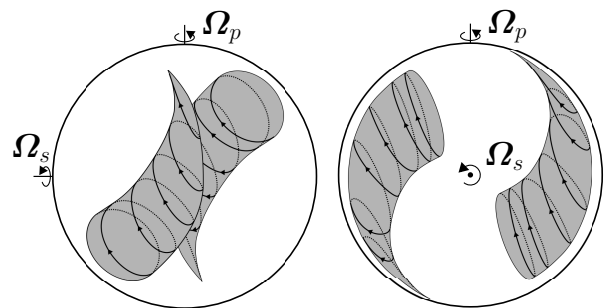

Figure 1. Precessing sphere.

Figure 2. Mean flow structure of the turbulence for $Po = 0.1$ and $Re = O(10^4)$. Schematic drawn on the basis of DNS of a Newtonian fluid. A pair of large-scale vortex tubes exists.

STRATEGY

Our strategy is the following: by investigating the statistics of turbulence of *non-Newtonian* fluids confined in a precessing sphere, we aim at understanding the sustaining mechanism of turbulence of a *Newtonian* fluid in it.

A small amount of surfactant or polymer additives can drastically change turbulence of water due to the viscoelasticity of the solutions. This interesting phenomenon is called Tom's effect for the case with polymer additives, in particular. The turbulence suppression has been extensively investigated because it provides an attractive technique of turbulence control (Virk, 1975; Berman, 1978; Zakin et al., 1988; White and Mungal, 2008). The physical mechanism of this phenomenon has also been investigated by many authors (e.g. Lumley, 1969, 1973; Tabor and de Gennes 1986; see also a recent review by White and Mungal, 2008). A key to the mechanism is the matching of the time-scales of turbulent eddies and the viscoelasticity of the solutions. Previous studies claim that once this matching occurs, eddies lose their kinetic energy because of the non-Newtonian viscosity or elasticity of the solutions. We emphasize that detailed investigation of the turbulence suppression can provide us with important information on the sustaining mechanism of turbulence because this phenomenon implies the inhibition of the mechanism due to the viscoelasticity.

As will be shown, a kind of surfactant additive indeed reduces the turbulence intensity in a precessing sphere. Note that we need to understand the physics of the sustainment of turbulence of a Newtonian fluid before we understand the mechanism of the modification of the examined turbulence. Systematic investigation of turbulence modification due to the additives, combined with the previous knowledge (i.e. the time-scale matching), therefore provides useful information to answer the question raised in the last paragraph of the previous section.

METHOD

We experimentally investigate the modification of turbulence in a precessing sphere by using the apparatus schematically shown in Fig. 3. We use an acrylic container with a spherical cavity whose radius is 90 mm. We drive the spin of the container on a rotating turntable to realize its precession. We visualize the flow using a laser sheet on the equatorial plane of the sphere. We conduct visualizations and PIV using aluminum flakes and nylon powders, respectively. A camera fixed on the turntable records the visualized
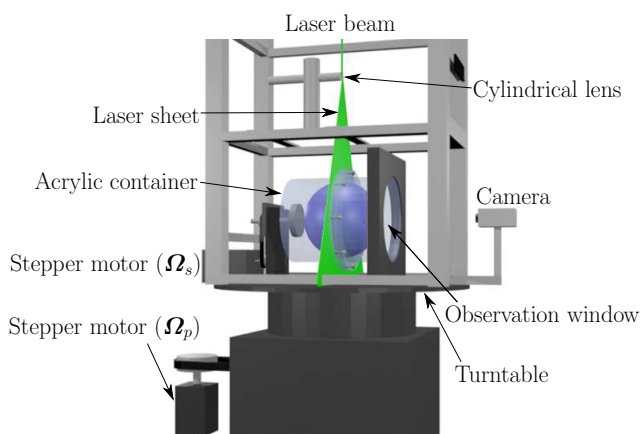
Figure 3. Experimental apparatus. The laser sheet always runs through the equatorial plane, and the flow state is recorded by a camera fixed on the turntable through the bottom "observation window" of the container. Its outer shape is cylindrical, whereas the cavity is a sphere with radius 90 mm.

flows.

We use a surfactant additive, cetyltrimethyl ammonium chloride (CTAC, 320.00 g/mol), with counterions, sodium salicylate (NaSal, 160.10 g/mol). The concentration of both of CTAC and NaSal is 50 wppm, which implies the molar ratio is 1:2. This surfactant solution exhibits viscoelasticity because thread-like micellar structures are formed in it (Wei et al., 2010). Since the solution is very dilute, we assume its zero-shear viscosity is the same as that of water, and we estimate the Reynolds number of the flows of the CTAC solution using the value of the kinetic viscosity of water at the same temperature.

During the experiments, we surrounded the apparatus with thermal insulators and circulated temperature-controlled air around the apparatus. This allows us to conduct experiments, which last over 10 hours, under the condition with a constant fluid temperature $(20 \pm 0.1 \,^{\circ}\text{C})$.

RESULTS

Small-scale eddies

Flake visualizations of turbulence of water and the CTAC solution are shown in Fig. 4 for $Re = 4.01 \times 10^4$ and $Po = 0.1$. Turbulence of the CTAC solution is much more quiescent than that of water, and small-scale vortices are drastically suppressed in the turbulence of the CTAC solution. For this Poincaré number ($Po = 0.1$), we observe the similar behavior for different Reynolds numbers in the range that $1.01 \times 10^4 \le Re \le 8.02 \times 10^4$. (Figures are omitted.)

To quantify the results of flow visualization, we investigate vorticity field on the equatorial plane in the sphere. We evaluate the vorticity by central difference of velocity fields obtained by using PIV. Figure 5 shows the temporal average of squared vorticity on the equatorial plane, which is normalized by the magnitude of spin angular velocity, of turbulence of (a–d) water and (e–h) the CTAC solution. The examined Reynolds numbers are (a, e) $Re = 1.01 \times 10^4$, (b, f) 2.03×10^4, (c, g) 4.01×10^4, and (d, h) 8.02×10^4, whereas the Poincaré number is fixed at $Po = 0.1$. Note that the squared vorticity reflects the intensity of small-scale vortices. It is clear in Fig. 5 that small-scale vortices are drastically suppressed in the bulk of turbulence of the CTAC solution and the region of the suppression gradually expands as the Reynolds number increases. For the highest Reynolds number, $Re = 8.02 \times 10^4$ [fig. 5(d, h)], the strong suppression occurs in the whole region except for top-right and bottom-left regions.

Large-scale eddies

Figure 6 shows the temporally-averaged velocity fields, obtained by using PIV, of turbulence of (a-d) water and (e-f) the CTAC solution. The examined parameters are the same as those in Fig. 5. In all the figures, the large-scale vortical structures are observed in
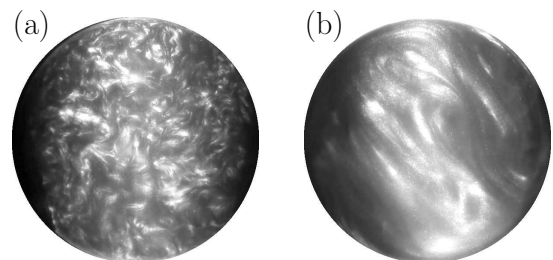
Figure 4. Flake visualization of turbulence of (a) water and (b) the CTAC solution (50 wppm). The parameters are common: $Re = 4.01 \times 10^4$ and $Po = 0.1$.
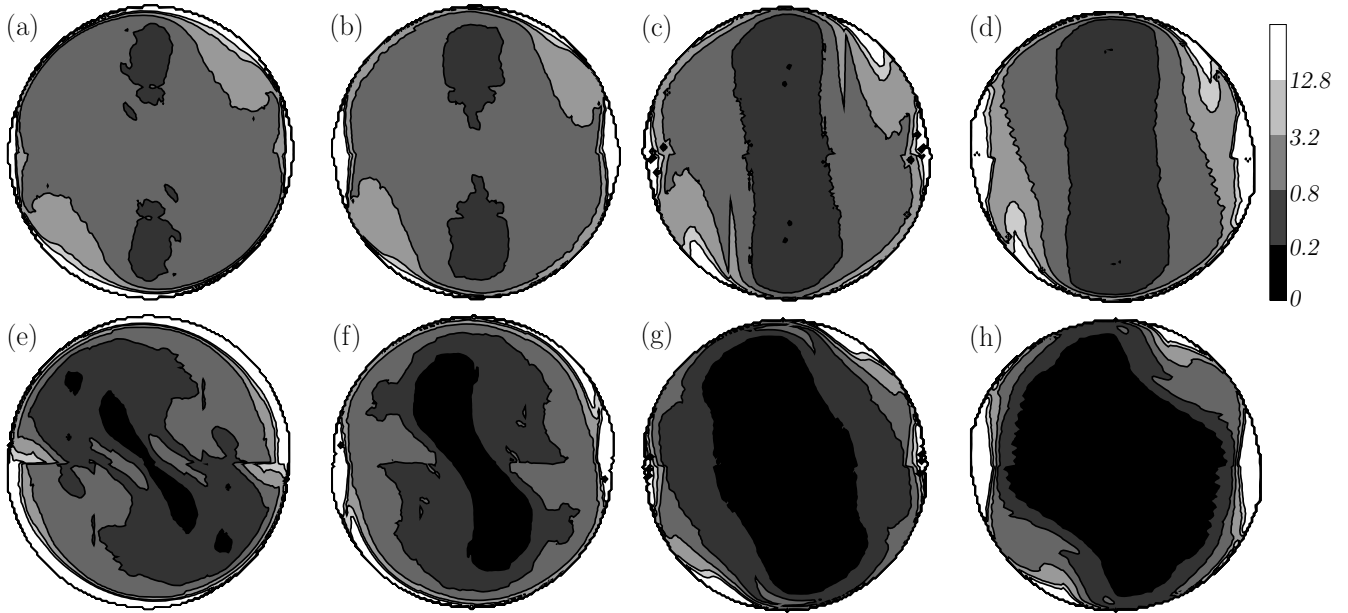
Figure 5. Temporal average of the squared vorticity on the equatorial plane of turbulence for $Po = 0.1$. (a-d) Water and (e-h) the CTAC solution (50 wppm). (a, e) $Re = 1.01 \times 10^4$, (b, f) 2.03×10^4, (c, g) 4.01×10^4, and (d, h) 8.02×10^4. Vorticity is normalized by the magnitude of the spin angular velocity, Ω_s.
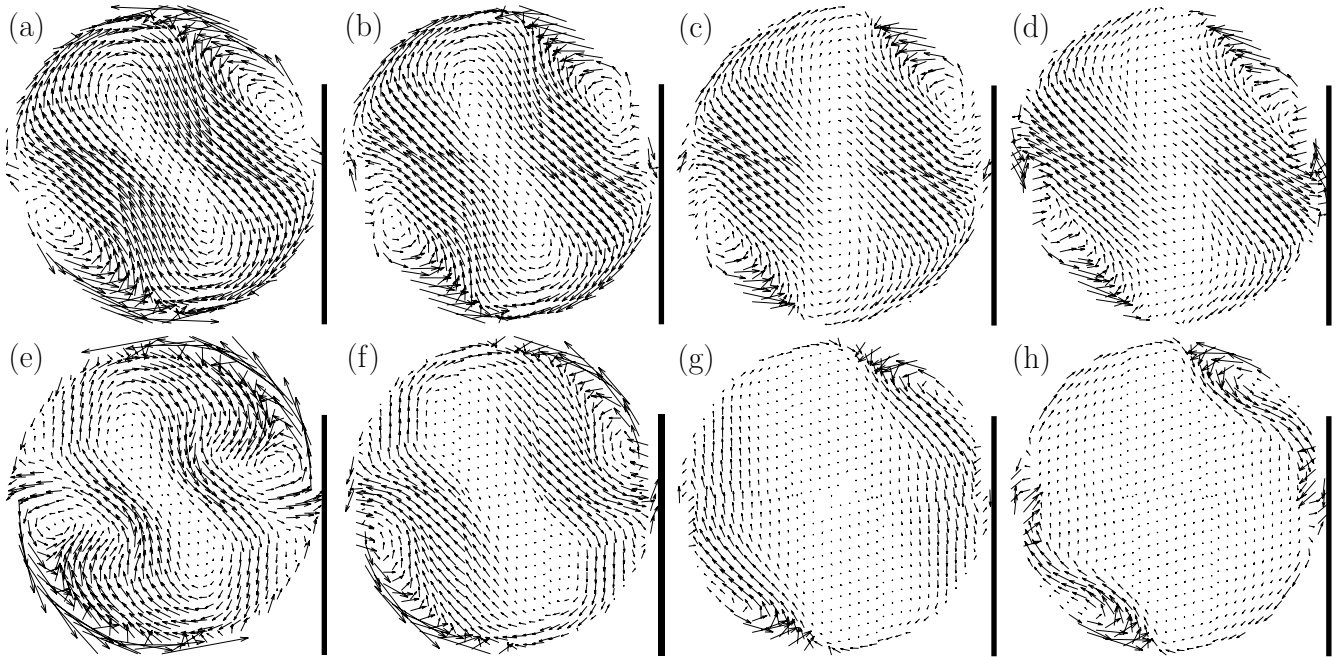

Figure 6. Temporally-averaged velocity field on the equatorial plane of turbulence for $Po = 0.1$. (a-d) Water and (e-h) the CTAC solution (50 wppm). (a, e) $Re = 1.01 \times 10^4$, (b, f) 2.03×10^4, (c, g) 4.01×10^4, and (d, h) 8.02×10^4. The thick vertical lines indicate the maximum speed of the wall, $a\Omega_s$.

the top-right and bottom-left regions. This implies that the pair of largest-scale vortex tubes (Fig. 2) survives even in the turbulence of the CTAC solution. On the other hand, in a central region of the sphere, large-scale shearing flow is suppressed in turbulence of the CTAC solution when the Reynolds number is relatively high, $Re = 4.01 \times 10^4$ [Fig. 6(c, g)] and 8.02×10^4 [Fig. 6(d, h)]. It is important that the region where the suppression occurs expands as the Reynolds number increases. We emphasize that for $Re = 4.01 \times 10^4$ and 8.02×10^4, the largest-scale vortex tubes in the top-right and bottom-left regions are also modified in their peripheries. This means that even the largest eddies in turbulence are affected by the viscoelasticity of the solution for relatively high Reynolds numbers because their time-scale matches with the characteristic time-scale of the viscoelasticity.
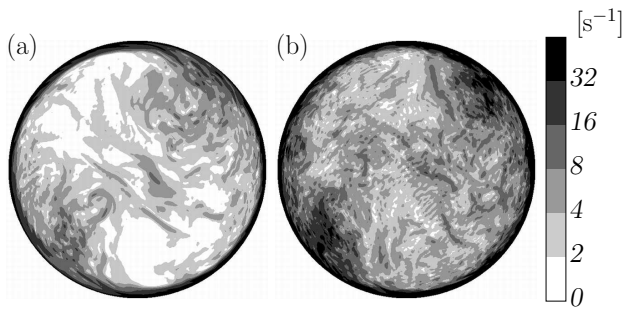
Figure 7. Instantaneous profile of shear rate in turbulence of a Newtonian fluid for $Po = 0.1$. DNS results for our experimental set-up ($a = 90$ mm and $\nu = 10^{-6}$ m^2/s). (a) $Re = 1 \times 10^4$ and (b) 2×10^4.

We have also verified by using the PIV data that turbulence intensity of the CTAC solution is suppressed in a central region of the sphere. The suppression of turbulence intensity shows the similar Reynolds-number dependence to that of the mean flow. (Figures are omitted.)

Furthermore, we have conducted the image analysis of the flow visualizations. More concretely, we calculate the temporal correlation function of the brightness at each point in visualized images to show that the temporal correlation for turbulence of the CTAC solution has much larger values than those of water. This result is consistent with the observed suppression of small-scale vortices in turbulence of the CTAC solution. (Figures are omitted, and to be presented in the conference together with other results, e.g. results for polymer solutions which have rheological properties different from the CTAC solution.)

DISCUSSION

There are at least two possibilities of the sustaining mechanism of small-scale vortices in the turbulence of a Newtonian fluid. In this section, we discuss these mechanisms and which one can explain our experimental results.

One possibility is that small-scale vortices are generated in a high-shear-rate region near the wall and advected by the large-scale vortex tubes (Fig. 2). Fluid motions observed in the flow visualizations seem to support this view, but the results of detailed measurements of turbulence of the CTAC solution deny this idea because it conflicts with the fact that the suppression of small-scale vortices occurs even when the large-scale vortex tubes exist (Fig. 6). Namely, once the large vortices exists, the advection of small-scale eddies must occur. Our results of flow visualization (Fig. 4) and PIV measurement (Fig. 5) show that there is no small-scale eddies in the bulk of the sphere, which implies that this mechanism is irrelevant.

The other possibility is that an energy cascading process starting from the largest-scale eddies (Fig. 2) generates small-scale vortices. This idea is consistent with the experimental observations. The characteristic time-scale of the viscoelasticity of a dilute CTAC solution is $O(0.1)$ s (Yu et al., 2004). By using DNS of turbulence of a Newtonian fluid, we calculate the shear rate, $\dot{\gamma}$. Figure 7 shows shear rate obtained by DNS of turbulence of a Newtonian fluid, which is defined by

$$\dot{\gamma} = \sqrt{s_{ij}s_{ij}}. \tag{3}$$

Here, s_{ij} is the strain rate tensor. We can confirm in Fig. 7 that the characteristic time of the CTAC solution is within the range of time-scales of the turbulent eddies under our experimental conditions. This is the reason why the kinetic energy of the vortices at a length scale where the time-scale matching occurs is transformed into the elastic energy or dissipated by non-Newtonian viscosity. Then, because the energy cascade is inhibited below this length scale, the smaller vortices do not exist.

This picture also explains the modification of mean velocity fields and its Reynolds–number dependence. In our experiments, the radius of the sphere (90 mm) and the kinematic viscosity of the confined fluids are fixed. Therefore, the increase of Re ($= a^2 \Omega_s / \nu$) corresponds to the increase of Ω_s. Since the time-scale of the flow is shorter for larger Ω_s, the time-matching scale is larger for higher Reynolds numbers. Larger vortices are therefore affected by the viscoelasticity, and this explains the Reynolds-number dependence observed in Fig. 6.

CONCLUSION

Our careful experiments, using non-Newtonian fluids, show that small-scale vortices in turbulence of a Newtonian fluid confined in a precessing sphere are created through an energy cascading process in the bulk region of the sphere and they are not created in the near-wall region. Although we have concentrated, in this paper, on the turbulence in a precessing sphere, our method using non-Newtonian fluids may be useful also for the investigation of the sustaining mechanism of other wall-bounded turbulent flows of Newtonian fluids.

REFERENCES

Malkus, W. V. R., 1968, "Precession of the Earth as the Cause of Geomagnetism," Science **160**, 259–264.

Le Bars, M., Cébron, D., & Le Gal, P., 2015, "Flows Driven by Libration, Precession, and Tides," Annual Review of Fluid Mechanics **47**, 163–193.

Goto, S., Matsunaga, A., Fujiwara, M., Nishioka, M., Kida, S., Yamato, M., & Tsuda, S., 2014a, "Turbulence driven by precession in spherical and slightly elongated spheroidal cavities," Physics of Fluids **26**, 055107.

Goto, S., Shimizu, M., & Kawahara, G., 2014b, "Turbulent mixing in a precessing sphere," Physics of Fluids **26**, 115106.

Virk, P. S., 1975, "Drag reduction fundamentals" AIChE Journal **21**, 625–656.

Berman, N. S., 1978, "Drag reduction by polymers," Annual Review of Fluid Mechanics **10**, 47–64.

Zakin, J. L., Bin, L., & Bewersdorff, H.-W., 1988, "Surfactant Drag Reduction," Reviews in Chemical Engineering **14**, 253–320.

White, C. M. & Mungal, M. G., 2008, "Mechanics and prediction of turbulent drag reduction with polymer additives," Annual Review of Fluid Mechanics **40**, 235–236.

Lumley, J. L., 1969, "Drag Reduction by Additives," Annual Review of Fluid Mechanics **1**, 367–384.

Lumley, J. L., 1973, "Drag reduction in turbulent flow by polymer additives," Journal of Polymer Science: Macromolecular Reviews **7**, 263–290.

Tabor, M., & P. G. de Gennes, 1986, "A cascade theory of drag reduction," Europhysics Letters **2**, 519–522.

Wei, J.-J., Kawagushi, Y., Yu, B., Li, F.-C., and Zhang, C.-W., 2010, "Microstructures and rheology of micellar surfactant solution by Brownian dynamics simulation," Nonlinear Dynamics **61**, 503-515.

Yu, B., Li, F.-C., & Kawaguchi, Y., 2004, "Numerical and experimental investigation of turbulent characteristics in a drag-reducing flow with surfactant additives," International Journal of Heat and Fluid Flow **25**, 961–974.